

The MBS Modelling of Structural Blade Offsets and its Impact on the Eigenbehaviour of Elastic Helicopter Rotors

Stefan Waitz

Institute of Aeroelasticity, DLR, Göttingen, Germany

Abstract

Since Multi Body System codes (MBS) have been proved to be potentially powerful simulation tools in the whole range of helicopter rotor dynamics, in this study the question of modelling the structural blade cross-section offsets in the MBS models is highlighted. The relative positions of the characteristic points of the cross-sections of helicopter blades like the shear center, the neutral axis and the cross-sectional center of gravity are formative for the dynamic behaviour of the rotating structure. Even the location of the reference point of the cross-section — which is defined by the radial connection between the hub and the cross-section, standing normal on the respective plane — plays an important role concerning the equilibrium of a rotating blade differential mass element. Although in helicopter blade design generally efforts are made to keep the offsets of these characteristic structural points small they can reach non-negligible extents and thus, together with the gyroscopic effects, contribute significantly to the coupling mechanisms between the motion components of the vibrating elastic blade structure like the flapping, lagging and torsional deformation. Also in terms of aeroelastic stability the cross-sectional offsets may have a dominant influence.

Here the scope of modelling blade offsets in MBS is to capture the complete variety of offsets resulting in the full range of mechanical coupling mechanisms like the bending-torsion coupling, the bending-longitudinal coupling and the bending-bending coupling (with “bending” meaning the flapping or lagging motion respectively). It is shown how special joint modelling techniques and the usage of “pseudo” bodies with additional DOF are introduced into the “pure” MBS model to reach this aim. The two basic approaches for incorporating elastic properties into a MBS model are addressed. The way of mapping the continuously distributed elastic properties of the blade beam structure on dynamic equivalent discrete spring stiffnesses of a “pure” MBS model is compared with FEM models which can be used as basis in the strategy of importing separately built up elastic Finite Element models with modal substructure techniques (FEMBS), thus resulting in a hybrid MBS model. While modelling of structural offsets within the pure MBS model refers to the genuine characteristics of the MBS modelling approach, the hybrid FEMBS model inherits all the advantageous (or deficient) properties of the incorporated Finite Element substructure. Since for the rotating blade the equilibrium state is now not only defined by the longitudinal normal forces but is three-dimensional, it is important for the geometric stiffness matrix S_g of the FEM formulation to contain the whole set of second order terms, while the cutting forces depend linear on the cross-sectional offsets and contribute linear to the geometric stiffness. Because the completeness of the FEM model constitutes the quality of the FEMBS solution by providing in particular the geometric stiffness matrix of the rotating blade, a separate FEM model has been analysed. On the MBS side the commercial tool SIMPACK has been tested while on the FEM side the inhouse tool GYRBLAD is used. As fully elastic single blade examples generic test beam cases with considerable offsets are used. The validation of the models is done by comparing the eigenvalue results produced with the two independent elasto-mechanical methods MBS and FEM.

1 Introduction

In recent time Multi Body System (MBS) codes have found their way into structural analysis within the helicopter industry, and the use of commercial MBS tools in the general design and development process seems to become common. These MBS codes combine not only their inherent property of describing large deflections of the (rigid) structure including full geometric non-linearities with in general high performance time integration algorithms. Furthermore in combination with special algorithmic features Finite Element Method (FEM) substructures can be incorporated into the MBS model replacing one or several rigid body components. By applying these so called FEMBS techniques consistent elastic and mass properties can be introduced into the structure to any desired amount. Together with these FEMBS structures and additional degrees of freedom added to the hybrid MBS model the complete dynamic model can be subjected to any kind of numerical simulation in time or frequency domain. Thus with MBS and FEM — which both have been applied in this study — two fundamentally different approaches in structural dynamics can be combined with their respective advantages to potentially high power CSD tools.

Since the most MBS codes have not primarily been designed for describing rotating elastic helicopter blades with their numerous potentially coupling mechanisms, in this paper these special features have been subjected to a systematic investigation to verify their correctness and reliability. The relative positions of the characteristic points of the cross-sections of helicopter blades like the shear center, the neutral axis and the cross-sectional center of gravity are formative for the dynamic behaviour of the rotating structure. Even the location of the reference radius of the cross-section — understood as the radial connection between the hub and the cross-section and standing normal on the respective plane — plays an important role concerning the equilibrium of the rotating blade differential mass element. Although in helicopter blade design generally efforts are made to keep the offsets of these characteristic structural points small they can reach non-negligible

extents and thus, together with the gyroscopic effects, contribute significantly to the coupling mechanisms between the deflection components of the vibrating elastic blade structure like the flapping, lagging and torsional deformation. Especially in terms of aeroelastic stability the cross-sectional offsets have a dominant influence.

While modelling of structural offsets within the “pure” MBS model refers to the genuine characteristics of the MBS modelling strategy plus specific offset modelling procedures, the FEM formulation necessitates the complete coupling mechanisms caused by the enlarged geometric stiffness properties — beside the establishing of the offset effects already for the non-rotating basic blade matrices. By implementing the FEM substructure the hybrid FEMBS model finally will inherit all the advantageous (or deficient) properties of the incorporated Finite Element model. In this study both approaches, the pure MBS and the pure FEM approach, will be applied to the different test beam cases. While the a priori linearised system matrices of the FEM formulation could directly be transferred into an eigenvalue problem, the stability analysis of the rotating MBS model requires additional working steps like establishing an equilibrium state and the linearisation of the equations of motion. It could be shown that one potential drawback of the MBS approach — the composition of the system matrices in a linearised equation of motion for the consecutive eigenvalue analysis — is successfully tackled with due to high performance differentiating algorithms.

In this study the commercial MBS code SIMPACK has been used and validated by comparisons to the FEM code GYRBLAD. The own in-house code GYRBLAD has primarily been designed for the 3-D motion of rotating beam like structures and contains the complete gyroscopic and geometric stiffness terms necessary to describe the spacial movement of a rotating elastic structure. The goal to keep a low error margin in the results to be compared to each other proved to be successful. Most of the eigenvalue results show a relative error of around 0.1%. To reach values further below this margin would have needed an additional major numerical effort in at least locally higher model resolution. On the other

hand error margins approaching or passing the 1% margin would have been a sign for probably wrong or incomplete physical modelling — on either of both sides to be compared.

2 Construction of the MBS model

As an example for a complex blade structure a complete MBS system rotating around the vertical hub axis is presented. Here its eigenbehaviour has been investigated in order to be compared with corresponding FEM solutions. (The basic structure and three eigenmodes of the rotating blade are to be seen in Fig. 2 and Fig. 11 until Fig. 13.) Each of the rigid bodies owns three-dimensional mass properties and originally the six DOF for the description of movement in space. The force interaction between the adjacent bodies as well as between the inner body and the rotation axis (hub) takes place by means of the stiffness of the applied springs. The stiffness values of the discrete springs are chosen in such a manner which will provide for the equivalent mechanical behaviour. For the longitudinal deformation the equivalent stiffness of tensile spring i will be

$$c_D^{equiv} = \frac{E_i A_i}{l_i}, \quad (1)$$

while for the two bending degrees of freedom in this section i an analogous expression is applied:

$$c_B^{equiv} = \frac{E_i I_i}{l_i}. \quad (2)$$

In contrast to the FEM modelling in the MBS model the two lateral DOF v_i and w_i are blocked and thus this system rotating with steady speed owns a number of DOF in total which is by one third smaller than the corresponding FEM model resolution. In the MBS model the lateral DOF are formulated as the angle deflections (relative) to the adjacent rigid body. For the MBS — as well as for the FEM formulation — the complete linearised equation of motion for the rotating system in general discretised degrees of freedom reads

$$\left(\left[\underline{K}_s \right] - \Omega^2 \left[\underline{K}_f \right] + \Omega^2 \left[\underline{K}_g \right] \right) \left\{ \underline{u} \right\} + 2\Omega \left[\underline{D}_g \right] \left\{ \dot{\underline{u}} \right\} + \left[\underline{M}_s \right] \left\{ \ddot{\underline{u}} \right\} = \left\{ \underline{0} \right\}. \quad (3)$$

The respective DOF of the MBS system are distributed in the deflection vector of the rotating blade as relative deformations, i.e. the deformation is measured relative to the (deformed) position of the adjacent bodies, whereas the FEM degree of freedoms are formulated in the classical manner as absolute deflections.

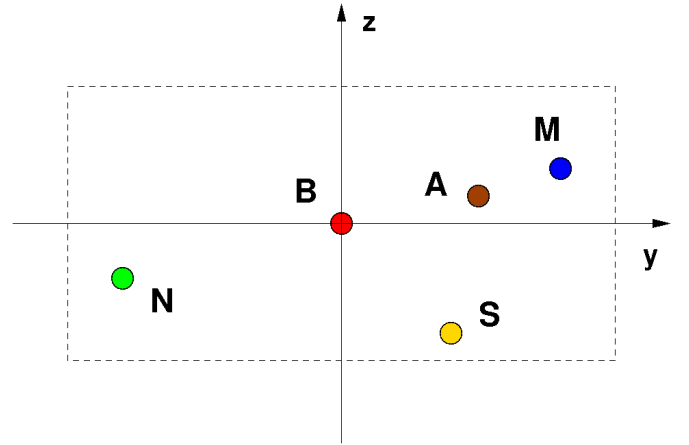


Figure 1: Scheme of the cross-section of the blade with offsets — M = Center of gravity; N = Structural neutral axis; S = Shear center; A = Aerodynamic neutral point; B = Pitch axis

A specific procedure was used to introduce the coupling effects between the respective DOF which were caused by the structural excentricities (offsets) of the cross-sectional characteristic points into the simulation model. For this purpose the complete possible offsets of the center of gravity (M), the neutral axis (N) and the shear center (S) in the two deflection coordinates y and z were introduced into the double-symmetric cross-section of the generic test blade. In addition the coupling effects caused by the pitching of the blade cross-section shall be included in the rotor model. As the reference point (B) for the offsets the radial beam (= pitch axis) between the rotor axis and the blade element, standing normal on the plane of the cross-section, is chosen (see Fig. 1). Of course a transformation of reference to other characteristic points like the aerodynamic neutral point is possible. The values of the introduced structural offsets are chosen in such a magnitude which allows the perception of their coupling effects in considerable extent but which still lies within

the range of applicability of the classical beam theory (small lateral system values with respect to the overall length).

Since in MBS between two neighbouring (rigid) bodies the deflections of the allowed degrees of freedom are situated in the position of the combining joint, primarily it proved to be impossible to introduce the wanted offsets. Thus a special procedure was applied and tested: By integrating an additional rigid body between two nominal blade-related bodies a second body joint could be created to allow for the spacial splitting of the degrees of freedom. These additional bodies exhibit no spacial extension in any direction with resulting zero mass properties, thus named as “pseudo” bodies. The total number of degrees of freedom remains constant for each blade body with the DOF being distributed between the two respective joints, one belonging to the real blade body and the other to the intermediate pseudo body. The splitting and distribution of the characteristic points to different excentric markers can be seen in Fig. 4.

The introduction of the excentricities into the joints together with a pitch inclination finally results in the ability to map the following stiffness and mass related coupling effects in the blade movement:

- flap-lag coupling
- flap-torsion and lag-torsion coupling
- flap-elongation and lag-elongation coupling

The coupling of the torsion-elongation movement should be possible in a similar manner but has not been activated yet. This complete rotating system is now subjected to an eigenvalue algorithm and the resulting numerical eigenfrequencies are compared to the numerical results achieved with a fundamentally different approach: On one hand the linearised MBS system of SIMPACK and on the other hand the FEM calculations with the code GYRBLAD. The values of the first 18 eigenfrequencies determined with the two methods are shown in Tab. 1 until Tab. 12 for the rotating as well as for the non-rotating blade systems. The displayed error margins are related to the 64 element FEM system and generally lie in the lower per mille range.

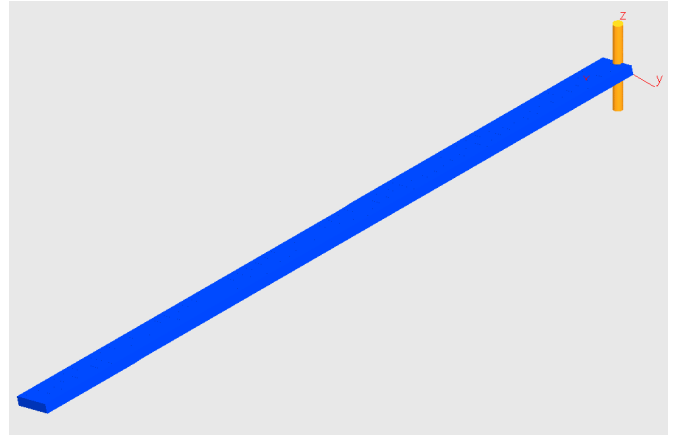


Figure 2: The 64 body MBS model: Joints modelled with equivalent discrete stiffnesses (15° pitch angle)

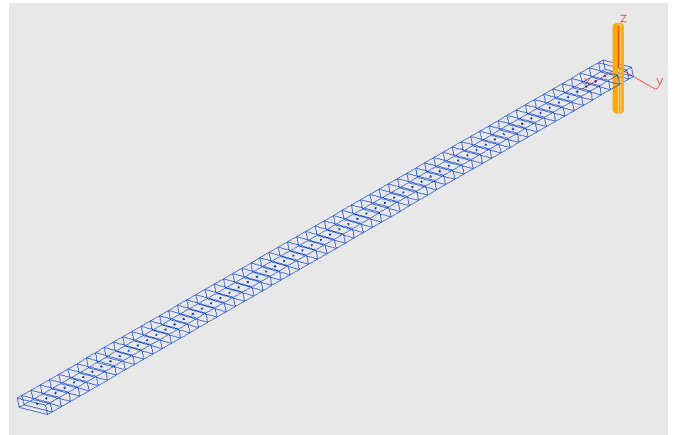


Figure 3: The 64 body MBS model: Combination of real blade and intermediate pseudo bodies (dotted)

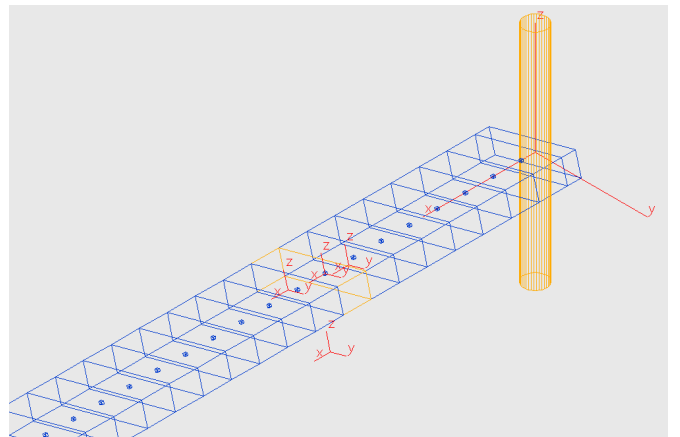


Figure 4: The 64 body MBS model: Excentric markers defining the cross-sectional point offsets of one blade body

3 The four test blade cases

Since in a prior investigation the focus had been put on the gyroscopic effects of the rotating blade structure without offsets [6], the same so called “Princeton beam” had been chosen as the basis for a generic elastic rotor beam. The original Princeton beam had been submitted to wide experimental testing and the results have been published in [1]. With its double symmetric cross-section any stiffness or mass coupling is excluded a priori and it is guaranteed for that a coupling between the various degrees of freedom in case of rotation originates only from the gyroscopic effects.

The original Princeton beam had a length of 20 [in] and a cross-section of 0.5×0.125 [in²]. Because of the aim of describing and validating the coupling of all possible DOF combinations a structural system had to be found where the longitudinal eigenmodes — at least one — lie sufficient low in the range of the system eigenvalues. That is one reason why for the numerical investigation here the length of the beam has been enlarged to 8 [m] and — by preserving the aspect ratios of the original Princeton beam — the cross-section was widened to 0.2×0.05 [m²]. Thus a model beam had been created which has the same material values and the same aspect ratios as the original Princeton beam but which is ~ 16 times enlarged in the external dimensions. The system values of this modified Princeton beam are defined as following:

$$\begin{aligned}
 l &= 8.0 && [\text{m}] ; \\
 b &= 0.20 && [\text{m}] ; && b/l = 2.5 [\%] ; \\
 h &= 0.05 && [\text{m}] ; && h/b = 25. [\%] ; \\
 \nu &= 0.33327 && [-] ; \\
 \rho &= 2796.0 && [\text{kg/m}^3] ; \\
 \eta &= 0.843 && [-] ; \\
 E &= 71.73 * 10^9 && [\text{N/m}^2] ; \\
 G &= 26.90 * 10^9 && [\text{N/m}^2] .
 \end{aligned}$$

To this enlarged Princeton beam another modification now was added by supplying the cross-sectional structural characteristic points with their respective offsets, thus creating a “new designed” blade structure exhibiting general anisotropic beam properties.

The values of the offsets are measured in the cross-sectional coordinate system, i.e. at “0° pitch angle”:

$$\begin{aligned}
 y_B \mid z_B &= 0.0 \quad | \quad 0.0 \quad [\text{m}] ; \\
 y_M \mid z_M &= 0.2 \quad | \quad 0.1 \quad [\text{m}] ; \\
 y_N \mid z_N &= -0.2 \quad | \quad -0.1 \quad [\text{m}] ; \\
 y_S \mid z_S &= 0.1 \quad | \quad -0.2 \quad [\text{m}] .
 \end{aligned}$$

Thus the respective offset values are 1.25 [%] and 2.50 [%] measured relatively to the blade length. Out of the named characteristics of the generic blade four test cases have been build up for the rotating blade and subjected to the eigenvalue analyses. The varied “modular components” have been the symmetric cross-section, the cross-sectional offsets and the pitch angle of the blade element, to be combined to the four blade test cases:

- (I.) Symmetric cross-section without pitch angle
- (II.) Symmetric cross-section with 15° pitch angle
- (III.) Cross-section with offsets and without pitch angle
- (IV.) Cross-section with offsets and with 15° pitch angle

It should be emphasised that from the structural dynamics point of view each of this four test blade models forms a distinct mechanical structure *sui generis*.

4 Convergence study of the MBS model

Both in the FEM model and in the MBS numeric model the rotating test blades have been divided into equidistant elements and bodies. Furthermore the beam and cross-section properties have been homogenously distributed over the blade length axis. This easily allowed separate calculations in advance in order to study the convergence behaviour of the simulation model and to answer the question of how many bodies or elements should be used to determine the lower (here: 18) system eigenmodes to a satisfying degree of accuracy.

SINGLE BLADE EIGENFREQUENCES [Hz] - CLAMPED, no OFFSETS, PITCH = 0 [o]

n = 0 [Hz]		SIMPACK (32 Bod.)		SIMPACK (64 Bod.)		SIMPACK (128 Bod.)		SIMPACK (extrap1.)	
1.)	1. Flap	0.6394	0.03 [%]	0.6393	0.02 [%]	0.6392	0.00 [%]	0.6392	0.00 [%]
2.)	1. Lag	2.5572	0.02 [%]	2.5567	0.00 [%]	2.5566	0.00 [%]	2.5566	0.00 [%]
3.)	2. Flap	4.0088	0.08 [%]	4.0065	0.02 [%]	4.0059	0.00 [%]	4.0057	0.00 [%]
4.)	3. Flap	11.2296	0.13 [%]	11.2189	0.03 [%]	11.2162	0.01 [%]	11.2153	0.00 [%]
5.)	2. Lag	16.0227	0.08 [%]	16.0134	0.02 [%]	16.0110	0.00 [%]	16.0102	0.00 [%]
6.)	4. Flap	22.0144	0.18 [%]	21.9850	0.04 [%]	21.9777	0.01 [%]	21.9753	0.00 [%]
7.)	5. Flap	36.4042	0.23 [%]	36.3424	0.06 [%]	36.3268	0.01 [%]	36.3215	-0.00 [%]
8.)	1. Tors	43.1652	-0.01 [%]	43.1684	-0.01 [%]	43.1692	-0.00 [%]	43.1695	-0.00 [%]
9.)	3. Lag	44.8335	0.13 [%]	44.7911	0.03 [%]	44.7805	0.01 [%]	44.7770	0.00 [%]
10.)	6. Flap	54.3979	0.27 [%]	54.2867	0.07 [%]	54.2584	0.02 [%]	54.2487	-0.00 [%]
11.)	7. Flap	75.9952	0.32 [%]	75.8157	0.08 [%]	75.7694	0.02 [%]	75.7533	-0.00 [%]
12.)	4. Lag	87.7485	0.17 [%]	87.6342	0.04 [%]	87.6056	0.01 [%]	87.5961	0.00 [%]
13.)	8. Flap	101.1930	0.36 [%]	100.9262	0.09 [%]	100.8558	0.02 [%]	100.8306	-0.00 [%]
14.)	9. Flap	129.3915	-0.07 [%]	129.4792	-0.00 [%]	129.5011	0.02 [%]	129.5084	0.02 [%]
15.)	2. Tors	129.9846	0.34 [%]	129.6141	0.06 [%]	129.5129	-0.02 [%]	129.4749	-0.05 [%]
16.)	5. Lag	144.7980	0.22 [%]	144.5635	0.05 [%]	144.5043	0.01 [%]	144.4843	-0.00 [%]
17.)	1. Long	158.2664	-0.01 [%]	158.2784	-0.00 [%]	158.2813	-0.00 [%]	158.2822	-0.00 [%]
18.)	10. Flap	162.3583	0.41 [%]	161.8742	0.11 [%]	161.7355	0.03 [%]	161.6798	-0.01 [%]

Table 1: MBS convergence study: Non-rotating symmetric blade ($n=0$ [Hz])

SINGLE BLADE EIGENFREQUENCES [Hz] - CLAMPED, no OFFSETS, PITCH = 0 [o]

n = 6 [Hz]		SIMPACK (32 Bod.)		SIMPACK (64 Bod.)		SIMPACK (128 Bod.)		SIMPACK (extrap1.)	
1.)	1. Lag	3.4219	0.25 [%]	3.4153	0.05 [%]	3.4136	0.00 [%]	3.4130	-0.01 [%]
2.)	1. Flap	6.2115	0.21 [%]	6.2017	0.05 [%]	6.1992	0.01 [%]	6.1983	-0.00 [%]
3.)	2. Flap	15.6052	0.26 [%]	15.5734	0.05 [%]	15.5653	-0.00 [%]	15.5625	-0.02 [%]
4.)	2. Lag	21.3044	0.14 [%]	21.2811	0.03 [%]	21.2752	0.00 [%]	21.2732	-0.01 [%]
5.)	3. Flap	27.0788	0.42 [%]	26.9904	0.09 [%]	26.9680	0.01 [%]	26.9604	-0.02 [%]
6.)	4. Flap	41.4999	0.60 [%]	41.3115	0.14 [%]	41.2640	0.02 [%]	41.2480	-0.02 [%]
7.)	1. Tors	43.5316	-0.01 [%]	43.5348	-0.01 [%]	43.5356	-0.00 [%]	43.5359	-0.00 [%]
8.)	3. Lag	51.1290	0.20 [%]	51.0508	0.05 [%]	51.0313	0.01 [%]	51.0248	-0.00 [%]
9.)	5. Flap	58.8210	0.77 [%]	58.4789	0.19 [%]	58.3928	0.04 [%]	58.3638	-0.01 [%]
10.)	6. Flap	79.1339	0.94 [%]	78.5755	0.23 [%]	78.4351	0.05 [%]	78.3879	-0.01 [%]
11.)	4. Lag	94.6720	0.25 [%]	94.4902	0.06 [%]	94.4447	0.01 [%]	94.4295	-0.00 [%]
12.)	7. Flap	102.5951	1.10 [%]	101.7531	0.27 [%]	101.5414	0.06 [%]	101.4703	-0.01 [%]
13.)	8. Flap	129.3398	1.24 [%]	128.1458	0.31 [%]	127.8450	0.07 [%]	127.7437	-0.01 [%]
14.)	2. Tors	129.5144	-0.11 [%]	129.6019	-0.05 [%]	129.6238	-0.03 [%]	129.6311	-0.02 [%]
15.)	5. Lag	152.0939	0.30 [%]	151.7493	0.07 [%]	151.6638	0.02 [%]	151.6356	-0.00 [%]
16.)	9. Flap	158.6094	0.82 [%]	157.8535	0.34 [%]	157.4454	0.08 [%]	156.9665	-0.22 [%]
17.)	1. Long	159.4665	0.53 [%]	158.6220	-0.00 [%]	158.6244	-0.00 [%]	158.6244	-0.00 [%]
18.)	10. Flap	193.0379	1.47 [%]	190.9452	0.37 [%]	190.4116	0.09 [%]	190.2290	-0.01 [%]

Table 2: MBS convergence study: Rotating symmetric blade with 0° pitch ($n=6$ [Hz])

SINGLE BLADE EIGENFREQUENCES [Hz] - CLAMPED, no OFFSETS, PITCH = 15 [o]

n = 6 [Hz]		SIMPACK (32 Bod.)		SIMPACK (64 Bod.)		SIMPACK (128 Bod.)		SIMPACK (extrap1.)	
1.)	1. Lag	3.3057	0.32 [%]	3.2976	0.07 [%]	3.2956	0.01 [%]	3.2949	-0.01 [%]
2.)	1. Flap	6.2741	0.19 [%]	6.2650	0.05 [%]	6.2627	0.01 [%]	6.2619	-0.00 [%]
3.)	2. Flap	15.5154	0.26 [%]	15.4834	0.05 [%]	15.4753	-0.00 [%]	15.4726	-0.02 [%]
4.)	2. Lag	21.3700	0.14 [%]	21.3468	0.03 [%]	21.3410	0.00 [%]	21.3391	-0.01 [%]
5.)	3. Flap	27.0332	0.42 [%]	26.9447	0.09 [%]	26.9223	0.01 [%]	26.9147	-0.02 [%]
6.)	4. Flap	41.4705	0.60 [%]	41.2820	0.14 [%]	41.2344	0.02 [%]	41.2183	-0.02 [%]
7.)	1. Tors	43.4827	-0.12 [%]	43.4859	-0.12 [%]	43.4867	-0.12 [%]	43.4870	-0.11 [%]
8.)	3. Lag	51.1534	0.20 [%]	51.0752	0.05 [%]	51.0557	0.01 [%]	51.0492	-0.00 [%]
9.)	5. Flap	58.8004	0.77 [%]	58.4581	0.19 [%]	58.3720	0.04 [%]	58.3431	-0.01 [%]
10.)	6. Flap	79.1185	0.94 [%]	78.5600	0.23 [%]	78.4196	0.05 [%]	78.3725	-0.01 [%]
11.)	4. Lag	94.6850	0.25 [%]	94.5033	0.06 [%]	94.4577	0.01 [%]	94.4424	-0.00 [%]
12.)	7. Flap	102.5832	1.10 [%]	101.7411	0.27 [%]	101.5294	0.06 [%]	101.4583	-0.01 [%]
13.)	8. Flap	129.3304	1.24 [%]	128.1364	0.31 [%]	127.8355	0.07 [%]	127.7341	-0.01 [%]
14.)	2. Tors	129.4979	-0.13 [%]	129.5854	-0.06 [%]	129.6073	-0.04 [%]	129.6146	-0.04 [%]
15.)	5. Lag	152.1018	0.30 [%]	151.7583	0.07 [%]	151.6715	0.02 [%]	151.6421	-0.00 [%]
16.)	9. Flap	158.6095	0.83 [%]	157.8459	0.34 [%]	157.4377	0.08 [%]	156.9689	-0.22 [%]
17.)	1. Long	159.4591	0.52 [%]	158.6207	-0.01 [%]	158.6248	-0.00 [%]	158.6248	-0.00 [%]
18.)	10. Flap	193.0316	1.47 [%]	190.9389	0.37 [%]	190.4052	0.09 [%]	190.2225	-0.01 [%]

Table 3: MBS convergence study: Rotating symmetric blade with 15° pitch ($n=6$ [Hz])

SINGLE BLADE EIGENFREQUENCIES [Hz] - CLAMPED, with OFFSETS, PITCH = 0 [o]

n = 0 [Hz]		SIMPACK (32 Bod.)		SIMPACK (64 Bod.)		SIMPACK (128 Bod.)		SIMPACK (extrap1.)	
1.)	1. Flap	0.6382	0.02 [%]	0.6381	0.00 [%]	0.6381	0.00 [%]	0.6381	0.00 [%]
2.)	1. Lag	2.4442	0.02 [%]	2.4438	0.00 [%]	2.4437	0.00 [%]	2.4437	0.00 [%]
3.)	2. Flap	3.9620	0.07 [%]	3.9598	0.02 [%]	3.9592	0.00 [%]	3.9590	-0.00 [%]
4.)	3. Flap	10.8716	0.10 [%]	10.8628	0.02 [%]	10.8606	0.00 [%]	10.8599	-0.00 [%]
5.)	2. Lag	12.4136	0.05 [%]	12.4101	0.03 [%]	12.4092	0.02 [%]	12.4089	0.02 [%]
6.)	4. Flap	20.8527	0.11 [%]	20.8335	0.02 [%]	20.8286	-0.01 [%]	20.8269	-0.02 [%]
7.)	3. Lag	28.2308	0.04 [%]	28.2389	0.07 [%]	28.2409	0.08 [%]	28.2416	0.08 [%]
8.)	5. Flap	33.4726	0.06 [%]	33.4485	-0.01 [%]	33.4424	-0.03 [%]	33.4403	-0.04 [%]
9.)	1. Tors	42.4055	-0.16 [%]	42.4741	0.00 [%]	42.4913	0.04 [%]	42.4971	0.06 [%]
10.)	6. Flap	48.2909	-0.06 [%]	48.2868	-0.07 [%]	48.2853	-0.07 [%]	48.2844	-0.07 [%]
11.)	2. Tors	50.8157	-0.22 [%]	50.9125	-0.03 [%]	50.9366	0.02 [%]	50.9446	0.04 [%]
12.)	4. Lag	62.6005	-0.13 [%]	62.8130	0.21 [%]	62.8658	0.30 [%]	62.8833	0.32 [%]
13.)	7. Flap	64.8069	-0.26 [%]	64.8844	-0.14 [%]	64.9025	-0.11 [%]	64.9080	-0.10 [%]
14.)	3. Tors	80.6371	-0.30 [%]	81.1163	0.30 [%]	81.2344	0.44 [%]	81.2730	0.49 [%]
15.)	8. Flap	82.3981	-0.54 [%]	82.6792	-0.20 [%]	82.7474	-0.12 [%]	82.7692	-0.10 [%]
16.)	9. Flap	94.5327	-0.66 [%]	95.3131	0.16 [%]	95.5069	0.36 [%]	95.5709	0.43 [%]
17.)	10. Flap	100.5647	-0.90 [%]	101.2184	-0.26 [%]	101.3758	-0.10 [%]	101.4257	-0.05 [%]
18.)	11. Flap	107.5394	-1.11 [%]	108.6175	-0.12 [%]	108.8870	0.13 [%]	108.9768	0.21 [%]

Table 4: MBS convergence study: Non-rotating blade with offsets ($n=0$ [Hz])

SINGLE BLADE EIGENFREQUENCIES [Hz] - CLAMPED, with OFFSETS, PITCH = 0 [o]

n = 6 [Hz]		SIMPACK (32 Bod.)		SIMPACK (64 Bod.)		SIMPACK (128 Bod.)		SIMPACK (extrap1.)	
1.)	1. Lag	2.4020	-5.36 [%]	2.4603	-3.06 [%]	2.4891	-1.93 [%]	2.5172	-0.82 [%]
2.)	1. Flap	6.2114	0.13 [%]	6.2039	0.00 [%]	6.2026	-0.02 [%]	6.2023	-0.02 [%]
3.)	2. Flap	14.3044	0.99 [%]	14.2367	0.52 [%]	14.2116	0.34 [%]	14.1968	0.23 [%]
4.)	2. Lag	17.2684	-0.41 [%]	17.2968	-0.25 [%]	17.3114	-0.16 [%]	17.3268	-0.07 [%]
5.)	3. Flap	25.5782	0.68 [%]	25.4769	0.28 [%]	25.4404	0.14 [%]	25.4198	0.06 [%]
6.)	3. Lag	32.5939	0.09 [%]	32.5736	0.03 [%]	32.5467	-0.05 [%]	32.6563	0.28 [%]
7.)	1. Tors	38.4812	0.34 [%]	38.4098	0.16 [%]	38.4075	0.15 [%]	38.4074	0.15 [%]
8.)	2. Tors	39.8333	0.21 [%]	39.8001	0.13 [%]	39.7697	0.05 [%]	39.4396	-0.78 [%]
9.)	4. Flap	48.4392	0.39 [%]	48.3350	0.17 [%]	48.2787	0.05 [%]	48.2125	-0.08 [%]
10.)	5. Flap	56.0735	-0.11 [%]	56.1512	0.02 [%]	56.1819	0.08 [%]	56.2020	0.11 [%]
11.)	6. Flap	63.5625	0.47 [%]	63.4452	0.28 [%]	63.3924	0.20 [%]	63.3492	0.13 [%]
12.)	7. Flap	72.6763	-0.05 [%]	72.8383	0.18 [%]	72.8805	0.24 [%]	72.8954	0.26 [%]
13.)	8. Flap	79.3314	0.19 [%]	79.3206	0.18 [%]	79.2887	0.14 [%]	79.3369	0.20 [%]
14.)	3. Tors	89.6046	-0.18 [%]	90.0391	0.30 [%]	90.1170	0.39 [%]	90.1340	0.41 [%]
15.)	9. Flap	94.3442	-0.85 [%]	94.8913	-0.27 [%]	95.0473	-0.11 [%]	95.1095	-0.04 [%]
16.)	10. Flap	99.0181	0.08 [%]	99.2328	0.29 [%]	99.2265	0.29 [%]	99.2267	0.29 [%]
17.)	11. Flap	108.8391	-1.01 [%]	109.9286	-0.02 [%]	110.1874	0.21 [%]	110.2680	0.29 [%]
18.)	12. Flap	114.8142	-0.29 [%]	115.4899	0.29 [%]	115.6636	0.44 [%]	115.7237	0.50 [%]

Table 5: MBS convergence study: Rotating blade with offsets and 0° pitch ($n=6$ [Hz])

SINGLE BLADE EIGENFREQUENCIES [Hz] - CLAMPED, with OFFSETS, PITCH = 15 [o]

n = 6 [Hz]		SIMPACK (32 Bod.)		SIMPACK (64 Bod.)		SIMPACK (128 Bod.)		SIMPACK (extrap1.)	
1.)	1. Lag	2.1628	-6.29 [%]	2.2267	-3.52 [%]	2.2596	-2.09 [%]	2.2945	-0.58 [%]
2.)	1. Flap	6.2214	-0.04 [%]	6.2185	-0.09 [%]	6.2190	-0.08 [%]	6.2189	-0.09 [%]
3.)	2. Flap	14.2375	0.93 [%]	14.1690	0.45 [%]	14.1429	0.26 [%]	14.1268	0.15 [%]
4.)	2. Lag	17.5486	-0.32 [%]	17.5737	-0.18 [%]	17.5774	-0.16 [%]	17.5780	-0.15 [%]
5.)	3. Flap	25.6181	0.62 [%]	25.5229	0.24 [%]	25.4921	0.12 [%]	25.4774	0.06 [%]
6.)	3. Lag	32.8510	0.08 [%]	32.8446	0.06 [%]	32.8302	0.02 [%]	32.8561	0.09 [%]
7.)	1. Tors	36.8475	0.19 [%]	36.7909	0.04 [%]	36.7405	-0.10 [%]	36.3308	-1.21 [%]
8.)	4. Flap	39.4641	0.36 [%]	39.3784	0.14 [%]	39.3761	0.14 [%]	39.3760	0.14 [%]
9.)	5. Flap	48.9125	0.31 [%]	48.8470	0.17 [%]	48.8078	0.09 [%]	48.7494	-0.03 [%]
10.)	6. Flap	55.6748	-0.10 [%]	55.7181	-0.02 [%]	55.7706	0.07 [%]	55.4710	-0.46 [%]
11.)	7. Flap	64.2662	0.41 [%]	64.2055	0.31 [%]	64.1297	0.20 [%]	64.5102	0.79 [%]
12.)	8. Flap	72.2755	-0.03 [%]	72.3964	0.14 [%]	72.4455	0.21 [%]	72.4791	0.25 [%]
13.)	9. Flap	80.0161	0.12 [%]	80.0834	0.20 [%]	80.0586	0.17 [%]	80.0653	0.18 [%]
14.)	2. Tors	89.1789	-0.25 [%]	89.5687	0.19 [%]	89.6764	0.31 [%]	89.7175	0.35 [%]
15.)	10. Flap	93.8436	-0.81 [%]	94.4350	-0.19 [%]	94.5802	-0.04 [%]	94.6275	0.01 [%]
16.)	11. Flap	98.9778	-0.00 [%]	99.2354	0.26 [%]	99.2134	0.24 [%]	99.2151	0.24 [%]
17.)	12. Flap	108.6397	-0.94 [%]	109.6630	-0.00 [%]	109.9744	0.28 [%]	110.1106	0.40 [%]
18.)	13. Flap	114.9879	-0.39 [%]	115.7666	0.29 [%]	115.8891	0.39 [%]	115.9120	0.41 [%]

Table 6: MBS convergence study: Rotating blade with offsets and 15° pitch ($n=6$ [Hz])

In this study three MBS models with different numbers of equidistant bodies have been built up and analysed: One coarse model with 32, one medium model with 64 and one model at a very fine discretisation level with 128 bodies have been used. Comparisons with the eigenvalues of the symmetric blade coming out of analytical solutions (Euler-Bernoulli-Beam) showed that for the lower ones out of the set of the analysed eigenvalues a global error margin of around one per mille could be reached already with the coarse model. As soon as cross-section offsets are integrated into the MBS model the accuracy of the solution turns significantly worse, both in the non-rotating and the rotating case. Especially the two lowest eigenvalues for the first flapping and the first lagging mode rise over 1%. Since the error magnitude of around 0.1% proved to be suitable also as a proof of the congruence of the physical model — i.e. the proof that all physically relevant components are integrated in the respective simulation model — the need of further assessment of the eigensolutions arose. With the help of the series of the three blade models with their increasing degree of model resolution it could be shown both a different convergence “speed” of the respective eigenvalues and by extrapolation — even more important — their common striving toward the correct limit values. Introducing the separate eigenvalues into the following homogenous extrapolation scheme,

$$(f_{i,\infty} - f_{i,32}) * a_i = (f_{i,64} - f_{i,32}) \quad (4)$$

$$(f_{i,\infty} - f_{i,64}) * a_i = (f_{i,128} - f_{i,64}), \quad (5)$$

this tendency could be clearly confirmed. Especially for the case of the first lagging eigenmode of the blade with offsets and the 15° pitch angle we can reach with $f_{1,\infty}$ a strongly improved eigenvalue result: From the coarse model value of 6.29% over the finer resolved models with the values of 3.52% and 2.09% to the finally extrapolated value of 0.58% error, see Tab. 6. (The error margins are defined by referring to the associated 64 element FEM blade model.) Of course this extrapolation scheme does not work reasonably for those eigenvalues where the accuracy of the numerical solution is reached already

at a lower resolution level (with low numerical noise).

A look at the corresponding eigenmodes discloses the evident reason for the different convergence behaviour and the low quality values for some of the eigenfrequencies: In occurs in those cases where (partially) strong gradients in the eigenmodes are present. This is especially the case for the 1. lagging mode of the above mentioned example, where in the modeshape very strong gradients in all (coupled) deflection components locally exist around the mounting region, which are unsufficiently resolved by the respective model solution order.

In comparison to the respective 64 element FEM blade model the error margins of the different cases, each with its quite different convergence behaviour — depending on the type of test blade being examined — are displayed in the Tab. 1 until Tab. 6.

5 Cutting forces and geometric stiffness

The rotational movement of the rotor blades of a helicopter in operation subjects the blade and hub structure to rotation specific loads which in general are very high and thus potentially operation limiting constraints. These acceleration effects are specially rotor speed dependent and may not be neglected in a dynamic simulation analysis under any circumstance. The gyroscopic effects as well as the geometric stiffening have an essential impact on the elastic blade and the complete H/C-rotor and influence their vibration behaviour significantly (see [6]). The eigenfrequencies and eigenmodes can change totally their amount and shape with respect to the rotation speed.

In particular the internal blade forces evoked by the centrifugal acceleration of the blade mass elements submitted to a homogenous rotation speed play a dominant role in the mechanic equilibrium of the structure. Beside their importance with respect to strength durability the cutting forces contribute also to the dynamic behaviour of the oscillating blade. In the cases of the symmetric cross-section with 0° pitch angle it is only the normal force varying along the blade axis which acts stiffening on the

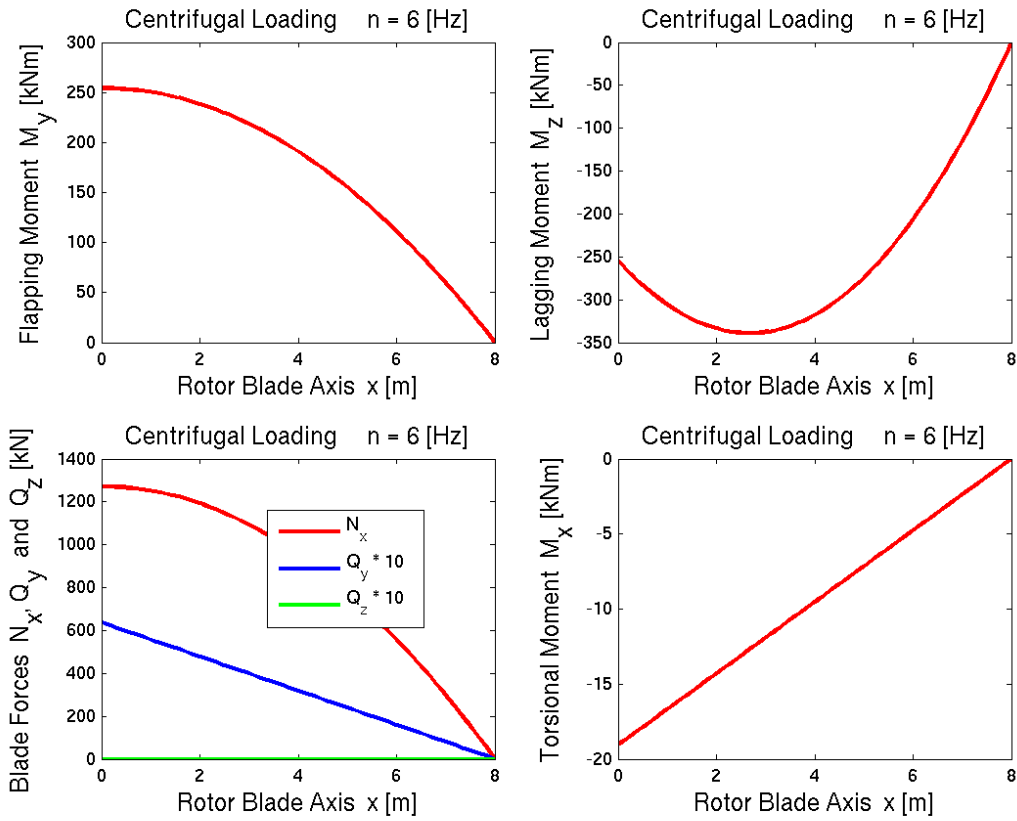


Figure 5: The cutting forces of the rotating blade with offsets and 0° pitch ($n=6$ [Hz])

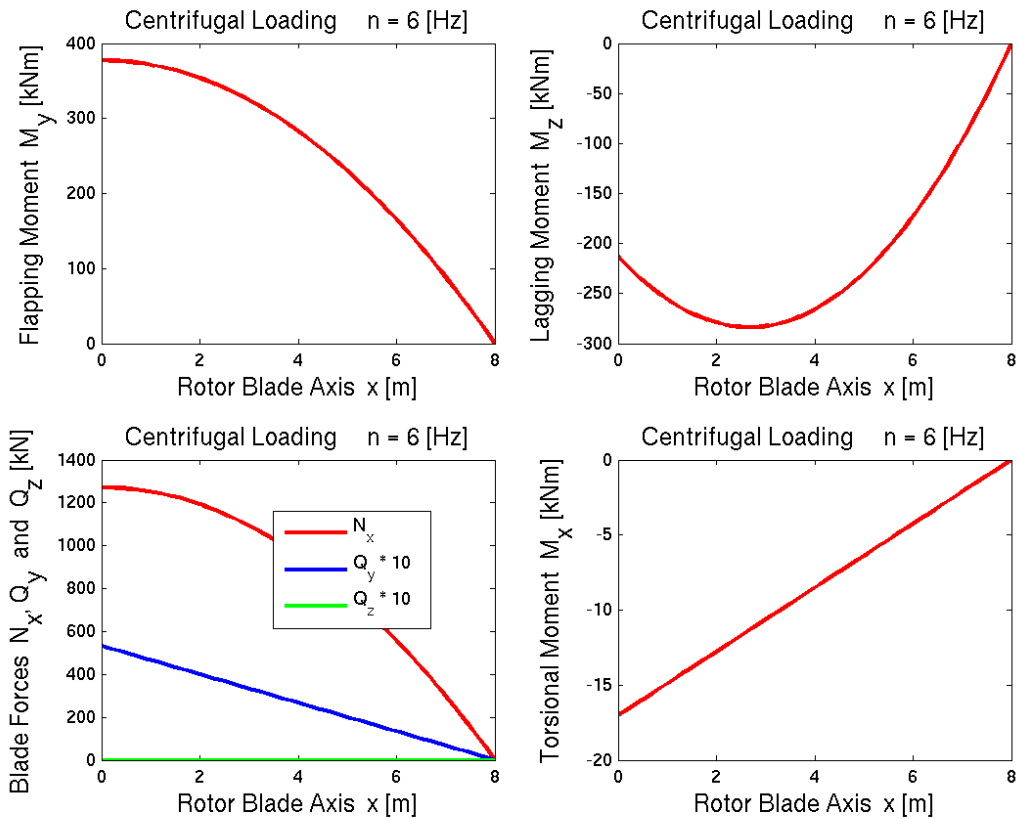


Figure 6: The cutting forces of the rotating blade with offsets and 15° pitch ($n=6$ [Hz])

eigenmodes. In the blade cases with cross-sectional offsets and pitch angles beside the dominant normal force we get a potentially fully specified vector of the cutting forces. Thus the need to incorporate these 3-D cutting forces into the geometric stiffness matrix arises. On side of the MBS modelling this is realised via corresponding equilibrium forces (“nominal forces”) whereas on the FEM side additional virtual energy expressions have to be formulated for the supplemental cutting forces. The final impact of the internal stress distribution may result in a stiffening as well as a softening of the structure.

In the Fig. 5 and Fig. 6 the cutting forces for the two offset blade cases with and without additional pitch angle are shown as result of the FEM calculations with GYRBLAD. Beside the unchanged normal force it can be seen that the two bending moments and the torsion moment as well as the lateral transverse force now are non zero. The vertical transverse force would contribute in case of aerodynamic lift and drag forces which here are neglected. While the torsional moment is caused only by transversal lateral acceleration of the cross-sectional mass distribution, the two bending moments are the result of the superimposed transversal and longitudinal acceleration generated by the blade rotation. The cutting moments shown in the graphs are displayed with respect to their corresponding characteristic points, i.e. the torsional moment with respect to the shear center and the two bending moments with respect to the neutral axis.

It can be seen that for the chosen set of cross-sectional offsets with an increasing of the pitch angle the flapping bending moment is rising whereas the lagging and the torsional moments are falling. (For the double symmetric cross-section — not displayed here — the torsional moment reaches its maximum values at 45° pitch angle.)

6 Numerical comparison of MBS with FEM results

Along with the MBS simulations all test blade cases have been analogously formulated with a finite element model and investigated parallel. Following

this strategy the two approaches could not only be tested and validated but also be compared simultaneously regarding precision and numerical reliability. Since the relative higher quality of the FEM solutions compared to the MBS solution with the same number of DOF — due to the capturing of the internal element strains by shape functions in FEM — only two FEM solution cases with 32 and 64 elements are presented here (against the three different MBS discretisations). In the Tab. 7 until Tab. 12 the respective eigenvalues are presented and confronted with the eigenvalues of the 64 and the 128 body MBS solutions. The error margins again are displayed with respect to the 64 element FEM solution (second double column). Beside the already above discussed disproportionate deviations in the eigenvalues for the first lagging mode of the rotating cross-sectional offset cases the agreement between the respective eigenvalues is as expected satisfying.

The single rotation speed eigenvalue solutions for the FEM as well as for the MBS blade model which here are displayed numerically — with $n = 6[\text{Hz}]$ — are contained in the presentation of the total frequency sweep in the fan diagrams of the eigenfrequencies in Fig. 7 until Fig. 10 as the second to last “x”-column.

7 Frequency fan diagrams of the single blade

Within a MBS algorithm the equations of motion in general are capable of describing arbitrarily large displacements of the individual rigid bodies which in turn are designed for the three-dimensional movement in a non-linear formulation. This implies that on one hand the complete mass tensor, crucial for capturing the rotation depending effects and defining the equilibrium state, is included in the simulation model. On the other hand there is the need to linearise the equations of motion prior to carrying out a stability analysis. This linearisation process which is obsolete in an a priori linearised and balanced Finite Element model requires high fidelity linearisation and equilibrating algorithms. The eigenvalue results compared in this study proved

SINGLE BLADE EIGENFREQUENCES [Hz] - CLAMPED, no OFFSETS, PITCH = 0 [o]

n = 0 [Hz]		GYRBLAD (32 E1m.)		GYRBLAD (64 E1m.)		SIMPACT (64 Bod.)		SIMPACT (128 Bod.)	
1.)	1. Flap	0.6392	0.00 [%]	0.6392	0.00 [%]	0.6393	0.02 [%]	0.6392	0.00 [%]
2.)	1. Lag	2.5566	0.00 [%]	2.5566	0.00 [%]	2.5567	0.00 [%]	2.5566	0.00 [%]
3.)	2. Flap	4.0057	0.00 [%]	4.0057	0.00 [%]	4.0065	0.02 [%]	4.0059	0.00 [%]
4.)	3. Flap	11.2154	0.00 [%]	11.2153	0.00 [%]	11.2189	0.03 [%]	11.2162	0.01 [%]
5.)	2. Lag	16.0103	0.00 [%]	16.0102	0.00 [%]	16.0134	0.02 [%]	16.0110	0.00 [%]
6.)	4. Flap	21.9754	0.00 [%]	21.9753	0.00 [%]	21.9850	0.04 [%]	21.9777	0.01 [%]
7.)	5. Flap	36.3226	0.00 [%]	36.3217	0.00 [%]	36.3424	0.06 [%]	36.3268	0.01 [%]
8.)	1. Tors	43.1738	0.01 [%]	43.1706	0.00 [%]	43.1684	-0.01 [%]	43.1692	-0.00 [%]
9.)	3. Lag	44.7771	0.00 [%]	44.7769	0.00 [%]	44.7911	0.03 [%]	44.7805	0.01 [%]
10.)	6. Flap	54.2521	0.01 [%]	54.2492	0.00 [%]	54.2867	0.07 [%]	54.2584	0.02 [%]
11.)	7. Flap	75.7624	0.01 [%]	75.7544	0.00 [%]	75.8157	0.08 [%]	75.7694	0.02 [%]
12.)	4. Lag	87.5968	0.00 [%]	87.5959	0.00 [%]	87.6342	0.04 [%]	87.6056	0.01 [%]
13.)	8. Flap	100.8521	0.02 [%]	100.8333	0.00 [%]	100.9262	0.09 [%]	100.8558	0.02 [%]
14.)	9. Flap	129.5210	0.03 [%]	129.4813	0.00 [%]	129.4792	-0.00 [%]	129.5011	0.02 [%]
15.)	2. Tors	129.6255	0.07 [%]	129.5393	0.00 [%]	129.6141	0.06 [%]	129.5129	-0.02 [%]
16.)	5. Lag	144.4883	0.00 [%]	144.4848	0.00 [%]	144.5635	0.05 [%]	144.5043	0.01 [%]
17.)	1. Long	158.2980	0.01 [%]	158.2861	0.00 [%]	158.2784	-0.00 [%]	158.2813	-0.00 [%]
18.)	10. Flap	161.7701	0.05 [%]	161.6933	0.00 [%]	161.8742	0.11 [%]	161.7355	0.03 [%]

Table 7: Comparison FEM with MBS: Non-rotating symmetric blade ($n=0$ [Hz])

SINGLE BLADE EIGENFREQUENCES [Hz] - CLAMPED, no OFFSETS, PITCH = 0 [o]

n = 6 [Hz]		GYRBLAD (32 E1m.)		GYRBLAD (64 E1m.)		SIMPACT (64 Bod.)		SIMPACT (128 Bod.)	
1.)	1. Lag	3.4146	0.03 [%]	3.4135	0.00 [%]	3.4153	0.05 [%]	3.4136	0.00 [%]
2.)	1. Flap	6.1988	0.00 [%]	6.1985	0.00 [%]	6.2017	0.05 [%]	6.1992	0.01 [%]
3.)	2. Flap	15.5739	0.05 [%]	15.5654	0.00 [%]	15.5734	0.05 [%]	15.5653	-0.00 [%]
4.)	2. Lag	21.2790	0.02 [%]	21.2747	0.00 [%]	21.2811	0.03 [%]	21.2752	0.00 [%]
5.)	3. Flap	26.9831	0.06 [%]	26.9661	0.00 [%]	26.9904	0.09 [%]	26.9680	0.01 [%]
6.)	4. Flap	41.2738	0.05 [%]	41.2544	0.00 [%]	41.3115	0.14 [%]	41.2640	0.02 [%]
7.)	1. Tors	43.5402	0.01 [%]	43.5370	0.00 [%]	43.5348	-0.01 [%]	43.5356	-0.00 [%]
8.)	3. Lag	51.0314	0.01 [%]	51.0264	0.00 [%]	51.0508	0.05 [%]	51.0313	0.01 [%]
9.)	5. Flap	58.3910	0.04 [%]	58.3705	0.00 [%]	58.4789	0.19 [%]	58.3928	0.04 [%]
10.)	6. Flap	78.4173	0.03 [%]	78.3949	0.00 [%]	78.5755	0.23 [%]	78.4351	0.05 [%]
11.)	4. Lag	94.4371	0.01 [%]	94.4313	0.00 [%]	94.4902	0.06 [%]	94.4447	0.01 [%]
12.)	7. Flap	101.5047	0.03 [%]	101.4777	0.00 [%]	101.7531	0.27 [%]	101.5414	0.06 [%]
13.)	8. Flap	127.7888	0.03 [%]	127.7523	0.00 [%]	128.1458	0.31 [%]	127.8450	0.07 [%]
14.)	2. Tors	129.7480	0.07 [%]	129.6603	0.00 [%]	129.6019	-0.05 [%]	129.6238	-0.03 [%]
15.)	5. Lag	151.6450	0.01 [%]	151.6364	0.00 [%]	151.7493	0.07 [%]	151.6638	0.02 [%]
16.)	9. Flap	157.3732	0.04 [%]	157.3180	0.00 [%]	157.8535	0.34 [%]	157.4454	0.08 [%]
17.)	1. Long	158.6410	0.01 [%]	158.6291	0.00 [%]	158.6220	-0.00 [%]	158.6244	-0.00 [%]
18.)	10. Flap	190.3332	0.05 [%]	190.2441	0.00 [%]	190.9452	0.37 [%]	190.4116	0.09 [%]

Table 8: Comparison FEM with MBS: Rotating symmetric blade with 0° pitch ($n=6$ [Hz])

SINGLE BLADE EIGENFREQUENCES [Hz] - CLAMPED, no OFFSETS, PITCH = 15 [o]

n = 6 [Hz]		GYRBLAD (32 E1m.)		GYRBLAD (64 E1m.)		SIMPACT (64 Bod.)		SIMPACT (128 Bod.)	
1.)	1. Lag	3.2964	0.03 [%]	3.2953	0.00 [%]	3.2976	0.07 [%]	3.2956	0.01 [%]
2.)	1. Flap	6.2624	0.01 [%]	6.2620	0.00 [%]	6.2650	0.05 [%]	6.2627	0.01 [%]
3.)	2. Flap	15.4839	0.05 [%]	15.4754	0.00 [%]	15.4834	0.05 [%]	15.4753	-0.00 [%]
4.)	2. Lag	21.3449	0.02 [%]	21.3406	0.00 [%]	21.3468	0.03 [%]	21.3410	0.00 [%]
5.)	3. Flap	26.9373	0.06 [%]	26.9204	0.00 [%]	26.9447	0.09 [%]	26.9223	0.01 [%]
6.)	4. Flap	41.2443	0.05 [%]	41.2249	0.00 [%]	41.2820	0.14 [%]	41.2344	0.02 [%]
7.)	1. Tors	43.5402	0.01 [%]	43.5370	0.00 [%]	43.4859	-0.12 [%]	43.4867	-0.12 [%]
8.)	3. Lag	51.0558	0.01 [%]	51.0508	0.00 [%]	51.0752	0.05 [%]	51.0557	0.01 [%]
9.)	5. Flap	58.3702	0.04 [%]	58.3497	0.00 [%]	58.4581	0.19 [%]	58.3720	0.04 [%]
10.)	6. Flap	78.4018	0.03 [%]	78.3794	0.00 [%]	78.5600	0.23 [%]	78.4196	0.05 [%]
11.)	4. Lag	94.4503	0.01 [%]	94.4445	0.00 [%]	94.5033	0.06 [%]	94.4577	0.01 [%]
12.)	7. Flap	101.4927	0.03 [%]	101.4657	0.00 [%]	101.7411	0.27 [%]	101.5294	0.06 [%]
13.)	8. Flap	127.7793	0.03 [%]	127.7428	0.00 [%]	128.1364	0.31 [%]	127.8355	0.07 [%]
14.)	2. Tors	129.7467	0.07 [%]	129.6618	0.00 [%]	129.5854	-0.06 [%]	129.6073	-0.04 [%]
15.)	5. Lag	151.6534	0.01 [%]	151.6448	0.00 [%]	151.7583	0.07 [%]	151.6715	0.02 [%]
16.)	9. Flap	157.3654	0.04 [%]	157.3102	0.00 [%]	157.8459	0.34 [%]	157.4377	0.08 [%]
17.)	1. Long	158.6409	0.01 [%]	158.6290	0.00 [%]	158.6207	-0.01 [%]	158.6248	-0.00 [%]
18.)	10. Flap	190.3268	0.05 [%]	190.2380	0.00 [%]	190.9389	0.37 [%]	190.4052	0.09 [%]

Table 9: Comparison FEM with MBS: Rotating symmetric blade with 15° pitch ($n=6$ [Hz])

SINGLE BLADE EIGENFREQUENCES [Hz] - CLAMPED, with OFFSETS, PITCH = 0 [o]

n = 0 [Hz]		GYRBLAD (32 E1m.)		GYRBLAD (64 E1m.)		SIMPACK (64 Bod.)		SIMPACK (128 Bod.)	
1.)	1. Flap	0.6381	0.00 [%]	0.6381	0.00 [%]	0.6381	0.00 [%]	0.6381	0.00 [%]
2.)	1. Lag	2.4437	0.00 [%]	2.4437	0.00 [%]	2.4438	0.00 [%]	2.4437	0.00 [%]
3.)	2. Flap	3.9592	0.00 [%]	3.9591	0.00 [%]	3.9598	0.02 [%]	3.9592	0.00 [%]
4.)	3. Flap	10.8619	0.01 [%]	10.8603	0.00 [%]	10.8628	0.02 [%]	10.8606	0.00 [%]
5.)	2. Lag	12.4083	0.01 [%]	12.4068	0.00 [%]	12.4101	0.03 [%]	12.4092	0.02 [%]
6.)	4. Flap	20.8409	0.05 [%]	20.8302	0.00 [%]	20.8335	0.02 [%]	20.8286	-0.01 [%]
7.)	3. Lag	28.2346	0.06 [%]	28.2185	0.00 [%]	28.2389	0.07 [%]	28.2409	0.08 [%]
8.)	5. Flap	33.4961	0.13 [%]	33.4527	0.00 [%]	33.4485	-0.01 [%]	33.4424	-0.03 [%]
9.)	1. Tors	42.5016	0.07 [%]	42.4730	0.00 [%]	42.4741	0.00 [%]	42.4913	0.04 [%]
10.)	6. Flap	48.4454	0.26 [%]	48.3184	0.00 [%]	48.2868	-0.07 [%]	48.2853	-0.07 [%]
11.)	2. Tors	50.9642	0.07 [%]	50.9266	0.00 [%]	50.9125	-0.03 [%]	50.9366	0.02 [%]
12.)	4. Lag	62.8393	0.25 [%]	62.6798	0.00 [%]	62.8130	0.21 [%]	62.8658	0.30 [%]
13.)	7. Flap	65.2740	0.46 [%]	64.9757	0.00 [%]	64.8844	-0.14 [%]	64.9025	-0.11 [%]
14.)	3. Tors	81.2246	0.43 [%]	80.8775	0.00 [%]	81.1163	0.30 [%]	81.2344	0.44 [%]
15.)	8. Flap	83.4321	0.70 [%]	82.8487	0.00 [%]	82.6792	-0.20 [%]	82.7474	-0.12 [%]
16.)	9. Flap	95.5311	0.38 [%]	95.1650	0.00 [%]	95.3131	0.16 [%]	95.5069	0.36 [%]
17.)	10. Flap	102.4831	0.99 [%]	101.4803	0.00 [%]	101.2184	-0.26 [%]	101.3758	-0.10 [%]
18.)	11. Flap	108.8903	0.13 [%]	108.7443	0.00 [%]	108.6175	-0.12 [%]	108.8870	0.13 [%]

Table 10: Comparison FEM with MBS: Non-rotating blade with offsets ($n=0$ [Hz])

SINGLE BLADE EIGENFREQUENCES [Hz] - CLAMPED, with OFFSETS, PITCH = 0 [o]

n = 6 [Hz]		GYRBLAD (32 E1m.)		GYRBLAD (64 E1m.)		SIMPACK (64 Bod.)		SIMPACK (128 Bod.)	
1.)	1. Lag	2.5401	0.08 [%]	2.5380	0.00 [%]	2.4603	-3.06 [%]	2.4891	-1.93 [%]
2.)	1. Flap	6.2041	0.01 [%]	6.2036	0.00 [%]	6.2039	0.00 [%]	6.2026	-0.02 [%]
3.)	2. Flap	14.1708	0.05 [%]	14.1636	0.00 [%]	14.2367	0.52 [%]	14.2116	0.34 [%]
4.)	2. Lag	17.3460	0.04 [%]	17.3395	0.00 [%]	17.2968	-0.25 [%]	17.3114	-0.16 [%]
5.)	3. Flap	25.4281	0.09 [%]	25.4049	0.00 [%]	25.4769	0.28 [%]	25.4404	0.14 [%]
6.)	3. Lag	32.5878	0.07 [%]	32.5644	0.00 [%]	32.5736	0.03 [%]	32.5467	-0.05 [%]
7.)	1. Tors	38.3650	0.04 [%]	38.3498	0.00 [%]	38.4098	0.16 [%]	38.4075	0.15 [%]
8.)	2. Tors	39.7778	0.07 [%]	39.7490	0.00 [%]	39.8001	0.13 [%]	39.7697	0.05 [%]
9.)	4. Flap	48.3311	0.16 [%]	48.2527	0.00 [%]	48.3350	0.17 [%]	48.2787	0.05 [%]
10.)	5. Flap	56.2372	0.18 [%]	56.1379	0.00 [%]	56.1512	0.02 [%]	56.1819	0.08 [%]
11.)	6. Flap	63.4262	0.25 [%]	63.2654	0.00 [%]	63.4452	0.28 [%]	63.3924	0.20 [%]
12.)	7. Flap	72.9122	0.28 [%]	72.7091	0.00 [%]	72.8383	0.18 [%]	72.8805	0.24 [%]
13.)	8. Flap	79.4956	0.40 [%]	79.1780	0.00 [%]	79.3206	0.18 [%]	79.2887	0.14 [%]
14.)	3. Tors	90.1134	0.38 [%]	89.7696	0.00 [%]	90.0391	0.30 [%]	90.1170	0.39 [%]
15.)	9. Flap	95.4635	0.33 [%]	95.1500	0.00 [%]	94.8913	-0.27 [%]	95.0473	-0.11 [%]
16.)	10. Flap	99.2646	0.32 [%]	98.9438	0.00 [%]	99.2328	0.29 [%]	99.2265	0.29 [%]
17.)	11. Flap	110.7696	0.74 [%]	109.9544	0.00 [%]	109.9286	-0.02 [%]	110.1874	0.21 [%]
18.)	12. Flap	116.0077	0.74 [%]	115.1530	0.00 [%]	115.4899	0.29 [%]	115.6636	0.44 [%]

Table 11: Comparison FEM with MBS: Rotating blade with offsets and 0° pitch ($n=6$ [Hz])

SINGLE BLADE EIGENFREQUENCES [Hz] - CLAMPED, with OFFSETS, PITCH = 15 [o]

n = 6 [Hz]		GYRBLAD (32 E1m.)		GYRBLAD (64 E1m.)		SIMPACK (64 Bod.)		SIMPACK (128 Bod.)	
1.)	1. Lag	2.3100	0.09 [%]	2.3079	0.00 [%]	2.2267	-3.52 [%]	2.2596	-2.09 [%]
2.)	1. Flap	6.2247	0.01 [%]	6.2242	0.00 [%]	6.2185	-0.09 [%]	6.2190	-0.08 [%]
3.)	2. Flap	14.1132	0.05 [%]	14.1061	0.00 [%]	14.1690	0.45 [%]	14.1429	0.26 [%]
4.)	2. Lag	17.6112	0.03 [%]	17.6052	0.00 [%]	17.5737	-0.18 [%]	17.5774	-0.16 [%]
5.)	3. Flap	25.4843	0.09 [%]	25.4614	0.00 [%]	25.5229	0.24 [%]	25.4921	0.12 [%]
6.)	3. Lag	32.8456	0.06 [%]	32.8250	0.00 [%]	32.8446	0.06 [%]	32.8302	0.02 [%]
7.)	1. Tors	36.7838	0.02 [%]	36.7768	0.00 [%]	36.7909	0.04 [%]	36.7405	-0.10 [%]
8.)	4. Flap	39.3630	0.10 [%]	39.3228	0.00 [%]	39.3784	0.14 [%]	39.3761	0.14 [%]
9.)	5. Flap	48.8374	0.15 [%]	48.7636	0.00 [%]	48.8470	0.17 [%]	48.8078	0.09 [%]
10.)	6. Flap	55.8302	0.18 [%]	55.7300	0.00 [%]	55.7181	-0.02 [%]	55.7706	0.07 [%]
11.)	7. Flap	64.1567	0.24 [%]	64.0044	0.00 [%]	64.2055	0.31 [%]	64.1297	0.20 [%]
12.)	8. Flap	72.5011	0.28 [%]	72.2967	0.00 [%]	72.3964	0.14 [%]	72.4455	0.21 [%]
13.)	9. Flap	80.2253	0.38 [%]	79.9233	0.00 [%]	80.0834	0.20 [%]	80.0586	0.17 [%]
14.)	2. Tors	89.7343	0.37 [%]	89.4028	0.00 [%]	89.5687	0.19 [%]	89.6764	0.31 [%]
15.)	10. Flap	94.8064	0.20 [%]	94.6144	0.00 [%]	94.4350	-0.19 [%]	94.5802	-0.04 [%]
16.)	11. Flap	99.4252	0.45 [%]	98.9794	0.00 [%]	99.2354	0.26 [%]	99.2134	0.24 [%]
17.)	12. Flap	110.4588	0.72 [%]	109.6671	0.00 [%]	109.6630	-0.00 [%]	109.9744	0.28 [%]
18.)	13. Flap	116.3056	0.75 [%]	115.4356	0.00 [%]	115.7666	0.29 [%]	115.8891	0.39 [%]

Table 12: Comparison FEM with MBS: Rotating blade with offsets and 15° pitch ($n=6$ [Hz])

to be quite sensitive to the respective algorithm and the accuracy of the linearisation process which can be selected in the eigensolution module of the MBS code SIMPACK (the best results achieved with the linearisation option: “optimal”).

Representing the case of fixed boundary conditions at a rigid hub the results for the clamped rotating single blade are shown in Fig. 7 until Fig. 10. With the two different methods MBS and FEM numerical calculations of the stability behaviour of the rotor and comparisons of the eigenvalues of the respective blades rotating at different speeds have been carried out with the codes SIMPACK and GYRBLAD. As result of the calculations for the rotating and the non-rotating four test cases the eigenvalues for the lower 18 eigenmodes are displayed numerically (see Tab. 1 until Tab. 12). The two above mentioned modelling methods MBS and FEM have been applied and their relative error margins — related to the 64 element GYRBLAD results — remain in the lower per mille range. For the symmetric cases the classification of the eigenmodes (for example in the zero pitch angle case: 10 flapping, 5 lagging, 2 torsion and 1 elongation mode) are quite evident, whereas the classification of the eigenmodes in the offset cases gets more difficult for the higher modes and/or with increasing rotor speed.

Already the (pure) MBS model built up with 32 rigid bodies shows a reasonable performance compared with the FEM formulation except for e.g. the high flapping modes of the rotating symmetric blade or the first mode of the blade with offsets where the error also reaches the 1% margin. In such cases the model resolution of the 32 rigid bodies proved to be insufficient for mapping of modes with high deflection gradients (e.g. higher modes with around 9 nodes and more).

In the fan diagrams of Fig. 7 until Fig. 10 the eigenfrequencies of the four test beam cases are shown with respect to the rotation speed of the rotor axis resulting from GYRBLAD FEM computations (in solid lines). Additionally displayed are the results from several distinct SIMPACK MBS calculations (marked with an “x” sign). It can be seen that the SIMPACK results lie well on the GYRBLAD

curves. The first 10 eigenfrequencies of the symmetric test beam with respect to rotor speed are shown in the fan diagram Fig. 7 and Fig. 8. There it can be seen that within the range of 70 [Hz] the first 10 eigenmodes comprise one torsional (43 [Hz]) (index letter “TT”) as well as 3 lagging and 6 flapping modes (index letters “YY” and “ZZ”) — with the first elongation mode (158 [Hz], index letters “XX”) lying outside this scope (see also Tab. 1 until 3). In the fan diagrams of Fig. 9 and Fig. 10 it can be seen at first glance that the eigenfrequencies of the test beam cases with cross-sectional offsets show lower values in comparison with the symmetric cases and thus exhibit a higher number of eigenmodes in the same frequency band until 70 [Hz]: 13 eigenmodes in the offset blade cases vs. 10 eigenmodes in the symmetric blade cases.

By applying an efficient mode tracking algorithm another important difference between the two blade classes could be examined. This gets apparent in the interacting of the eigenmodes for which their “crossing behaviour” among each other is a clear criterion. In the case of the symmetric blade with 0° pitch angle every eigenfrequency branch seems to be independent in crossing all other branches lying “on its way”. Increasing the pitch angle from 0° to 15° leads to the effect that the first lagging and the first flapping modes do not cross any longer but are bent around the original crossing point. This phenomenon becomes even more evident in the test blade cases with offset (see Fig. 9 and Fig. 10). Among the displayed frequency branches none is crossing each other any longer. By increasing the pitch angle the effect again is intensified: The frequency branches which still seem to have been “touching” each other are now moving apart (see eigenmodes 1 with 2 and eigenmodes 10 with 11 in Fig. 9 and Fig. 10). The reason for this behaviour lies in the very strong coupling between the different components of the eigenvectors. Although in the symmetric cross-section cases there occurs very strong component coupling between special degrees of freedom at certain rotation speeds (the “gyroscopic resonance”, see [6]), in all the cases of mass and stiffness related cross-section offset coupling the interaction between the deflection components flap-

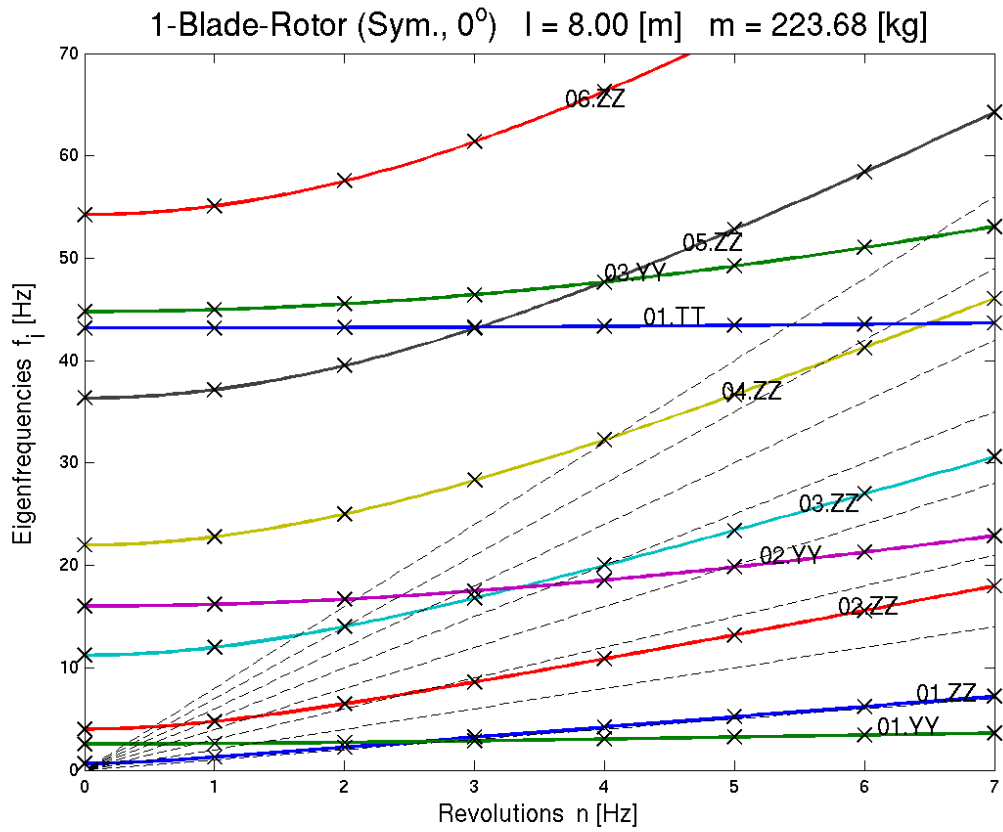


Figure 7: The first 10 eigenfrequencies of the symmetric blade with 0° pitch (FEM: —, MBS: x)

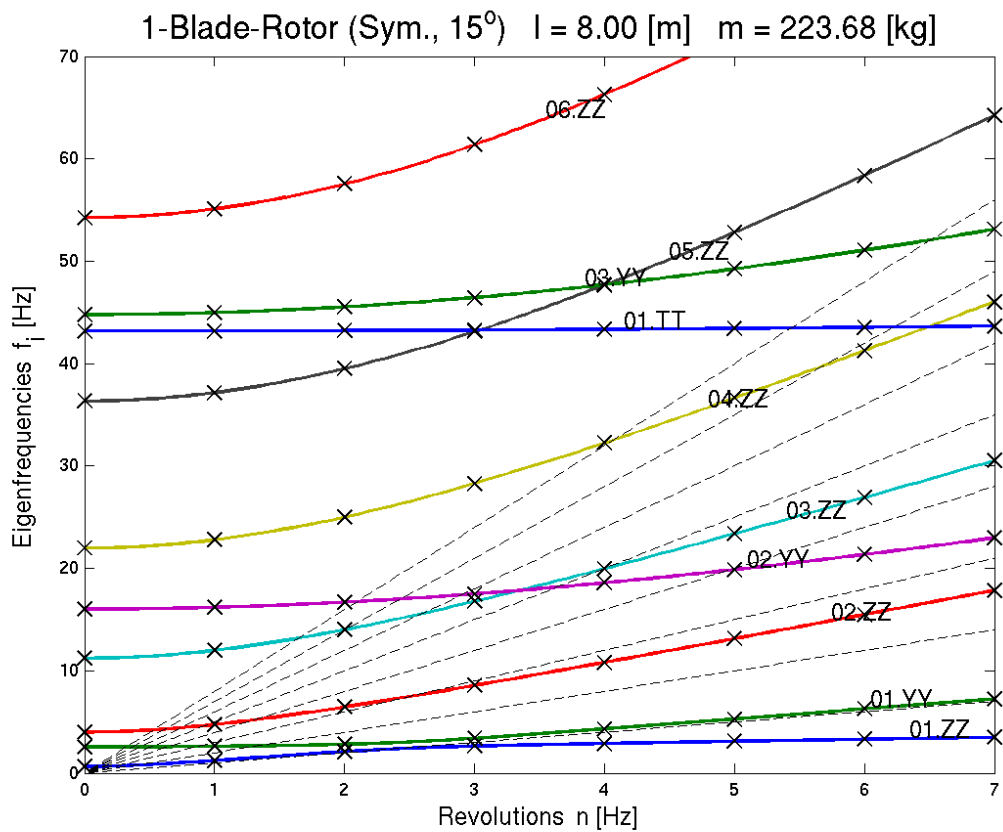


Figure 8: The first 10 eigenfrequencies of the symmetric blade with 15° pitch (FEM: —, MBS: x)

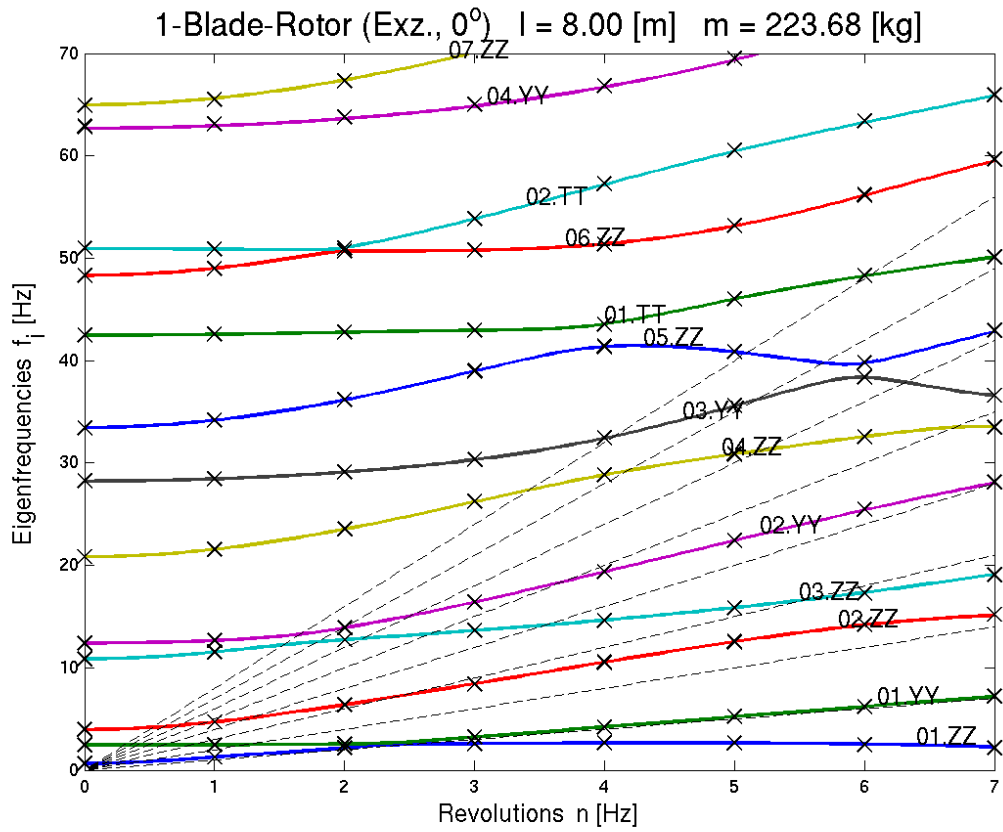


Figure 9: The first 13 eigenfrequencies of the blade with offsets and 0° pitch (FEM: —, MBS: x)

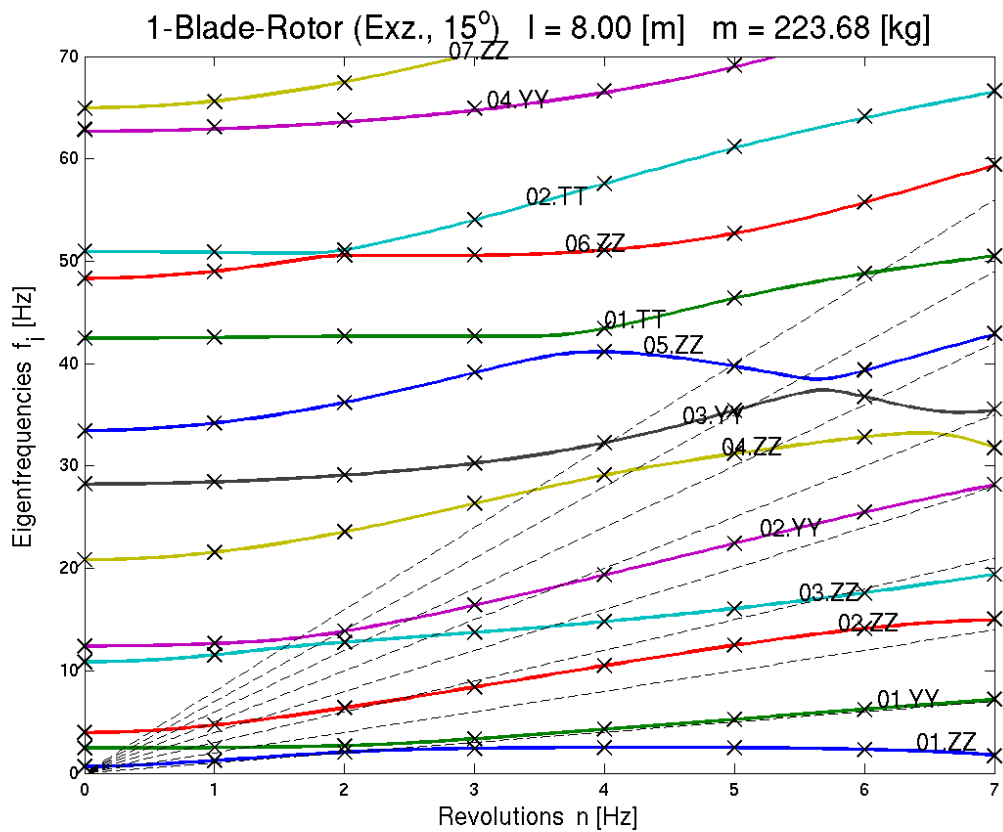


Figure 10: The first 13 eigenfrequencies of the blade with offsets and 15° pitch (FEM: —, MBS: x)

ping, lagging, stretching and torsion is more intensive and concerns each single eigenmode.

The rotation of the elastic blade causes a coupling between the components of the eigenvectors which in the non-rotating state — in case of the double symmetric cross-section — have been uncoupled. Although with increasing rotor speed the coupling effect gets stronger the time delayed (imaginary) fraction of the eigenmodes remain relatively small as long as the blade is built up by a long and slender beam without offsets. Looking at the variation of the eigenmodes with increasing rotor speed, mode specific regions then can be detected where the gyroscopically coupled components display a steep rise. (Exceeding the nominal components they strive to infinity and — after changing sign — they attenuate again.) These resonance-like effects between the gyroscopically coupled components occur at specific rotor speeds and frequencies at the intersection points of the eigenfrequency branches, see also [6]. Looking at the frequency curves of the involved eigenmodes with offsets (see in Fig. 9 and Fig. 10 e.g. the first torsion mode “1.TT” and the fifth flapping mode “5.ZZ”) one can not only perceive the formerly distinct resonance (crossing) point; it also is evident that in the adjacent frequency regions before and behind the resonance point an intense coupling with large coupled component fractions occur. At least the frequency bands of rotor speed of such areas seem to be more or less confined.

8 The eigenmodes of the rotating blade with offsets

The main impact of the gyroscopic terms on the dynamic behaviour of the rotating structure in general can be described as a coupling of (previously uncoupled) degrees of freedom. The eigenmodes — even of an originally undamped system — become complex and the eigenfrequencies will either be lifted or lowered. In the case of the presence of double eigenfrequencies previously equal frequencies will be split up. The apparent gyroscopic effects can be classified not only formally as contributions to the damping (antisymmetric matrix) and the stiffness terms of

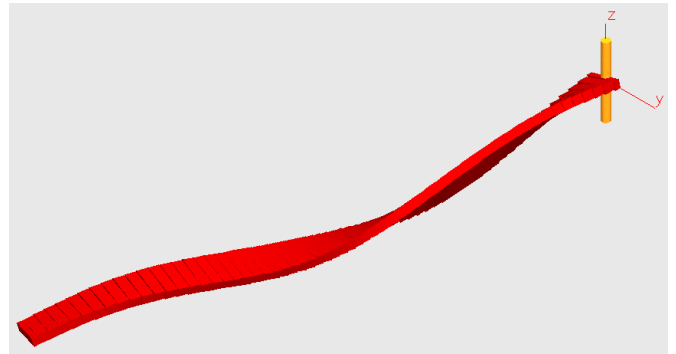


Figure 11: MBS: The 6th eigenmode of the blade with offsets and 15° pitch ($n=6[\text{Hz}]$)



Figure 12: MBS: The 8th eigenmode of the blade with offsets and 15° pitch ($n=6[\text{Hz}]$)

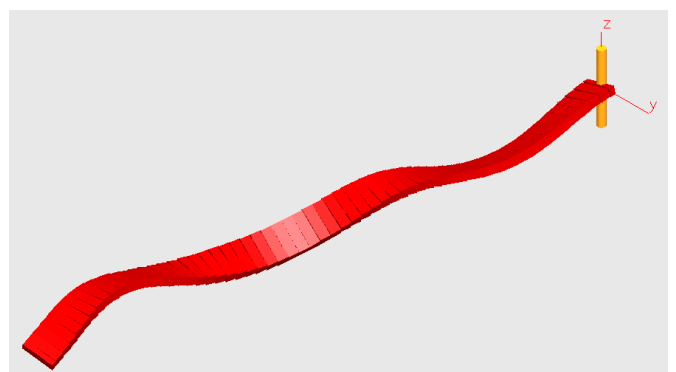


Figure 13: MBS: The 10th eigenmode of the blade with offsets and 15° pitch ($n=6[\text{Hz}]$)

the equation of motion (with either stiffening or softening impact) but also physically as mass phenomena which arise either from the deformation of the vibrating structure or the radius dependent position along the rotating blade axis (geometric stiffness). All these physical phenomena here apply as well for the rotating rigid body MBS model as for the elastic structure of the continuously flexible FEM rotor.

In contrast to a (technological) unsymmetric blade the double symmetric cross-section of the beam without any cross-sectional offsets and pitch angle is of advantage in the case of studying DOF coupling as a result only from rotation because it allows the focus on the pure gyroscopic coupling. On the other hand all other possible coupling mechanisms of an arbitrary real structure like coupling by mass or stiffness — here the aerodynamic forces are not included — are accounted for in the presented blade models with offsets and pitch angle — which on their part indeed influence the behaviour of the vibrating real rotor blades to a remarkable extent. The “multi component” cross-sectional offset induced coupling of the blade deflections is superimposed by the pure gyroscopic coupling of the flapping-torsion and the lagging-stretching components.

For the purpose of easier analysing the eigenmodes in Fig. 14 until Fig. 17 the FEM results of GYRBLAD calculations have been displayed in four separated subdiagrams for one component of the nodal displacements each (i.e. the flapping, lagging, stretching and the torsional component). Although the composition of every eigenmode changes with the rotation speed to take shape in any order, the main characteristics of the gyroscopic coupling here still can be observed in the time delay of the coupling of the DOF. The pure coupling classes “flapping-torsion” and “lagging-stretching” as to be observed in the double-symmetric cross-section case does not exist any longer, instead all components are coupled with each other.

The presented eigenmodes belong to the $n = 6$ [Hz] rotor speed and refer to the rotating offset and pitch angle cases which are presented above in Tab. 6 and Tab. 12. In the SIMPACK MBS pictures the

spacial character of the movement of the oscillating blade is captured whereas in the GYRBLAD FEM diagrams the equal magnitude of the offset coupled degrees of freedom gets evident. In Fig. 14 until Fig. 17 the four eigenmodes No. 5, 6, 7 and 8 at the same rotating speed $n = 6$ [Hz] are presented, each one for a different “main” (nominal) deflection component being dominant. The stereoscopic illustration of three respective MBS eigenmodes (the 6., 8. and 10. eigenmode) out of the SIMPACK calculations can be seen in Fig. 11 until Fig. 13.

In all studied eigenmodes of the fully coupled offset cases the torsional component plays a dominant role. Concerning the blade aerodynamics especially the torsional movement is highly relevant. While the aerodynamic forces are sensitive already to minor changes of the pitch angles the blade pitch amplitude rises to very large values not only in the gyroscopic resonance areas. Even for the slim and slender beam with high aspect ratio which has been investigated here — and how H/C blades use to be like — this effect is potentially dangerous with respect to the coupled flapping/torsional movement and the role it plays in aeroelastic stability. Containing the complete mass and stiffness driven coupling effects in addition to the gyroscopic ones, for a real aeroelastic rotor system with offsets a not at all negligible coupling especially in the blade pitch movement has to be stated. For the aeroelastic stability analysis of the rotating elastic helicopter blades these rotational effects may mean a favourable, i.e. damping, or a contrary, highly exciting influence.

9 Conclusions

The main topics of this investigation have been:

- Modelling the cross-sectional structural offsets of rotating H/C blades with advanced CSD tools like the MBS code SIMPACK,
- studying the impact of rotation on the dynamic behaviour of the offset coupled structure and
- validating the results of the MBS eigenvalue analysis by comparing them with results from a different method and independent code (FEM).

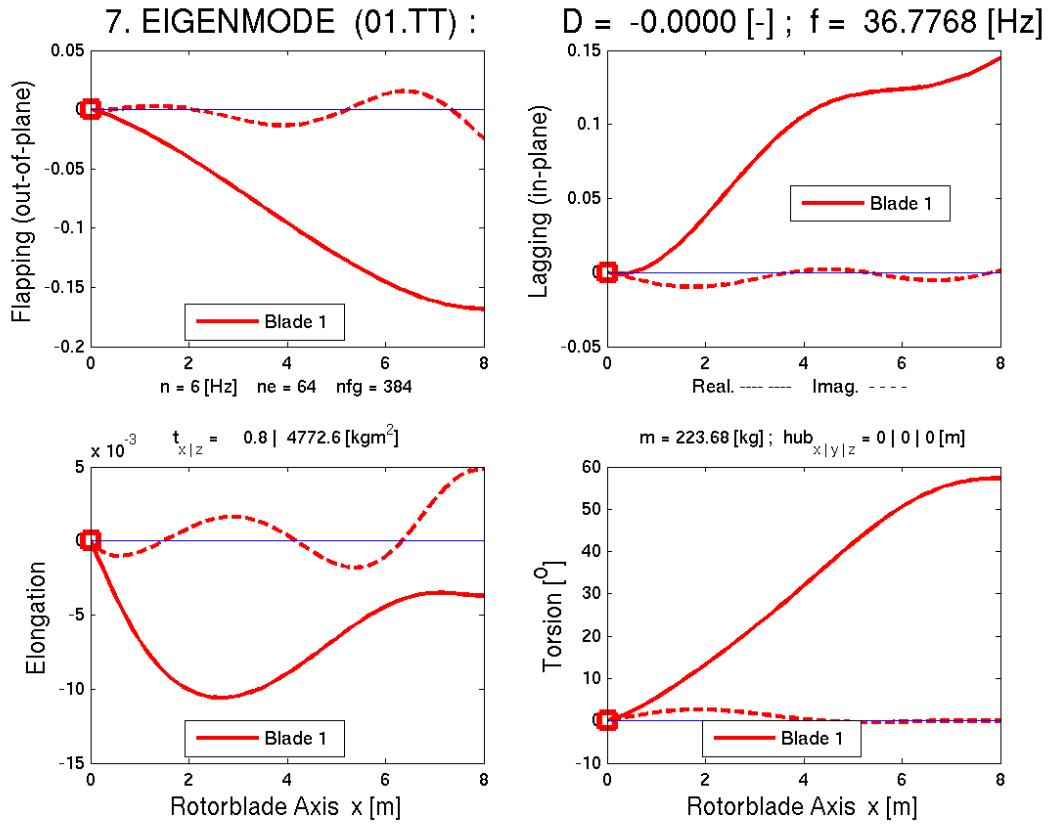


Figure 16: FEM: Components of the 7th eigenmode of the blade with offsets and 15° pitch ($n=6[Hz]$)

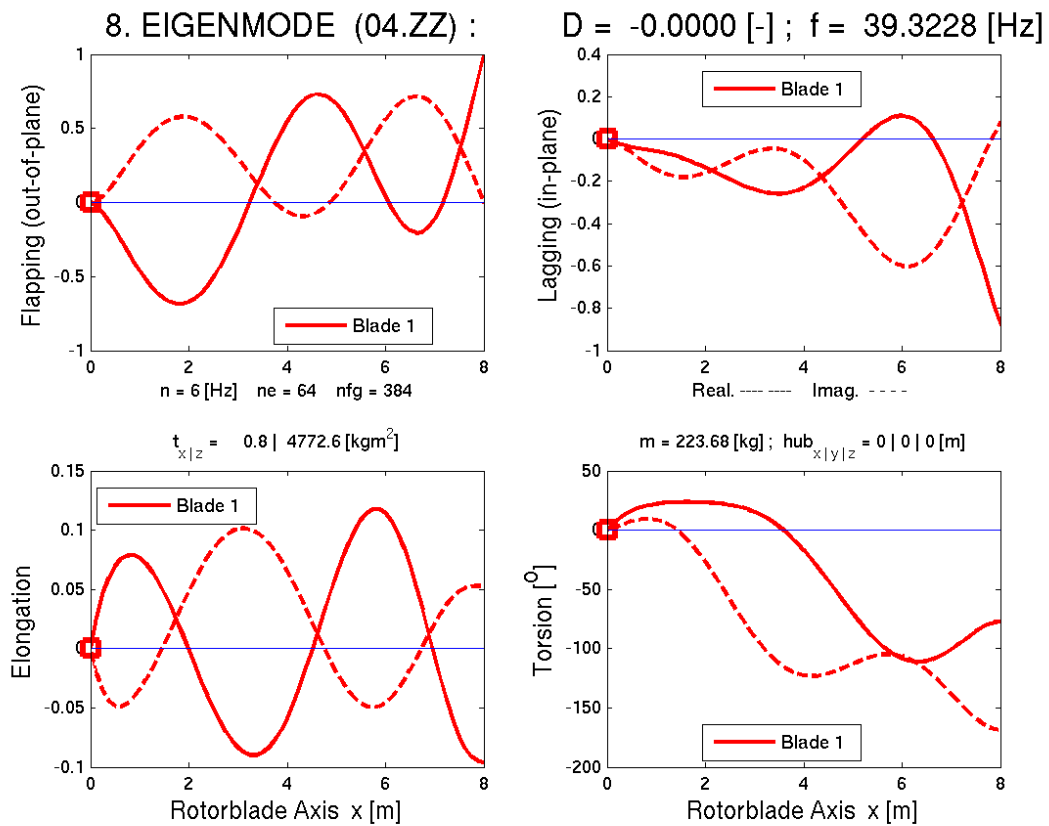


Figure 17: FEM: Components of the 8th eigenmode of the blade with offsets and 15° pitch ($n=6[Hz]$)

The analysis covered a full elastic rotating 8 [m] generic blade based on a modified — in size and cross-sectional offsets — Princeton beam with different structural offset and pitch angle conditions. For the computation of the eigenbehaviour it had been made use of the in-house FEM code GYRBLAD and the rigid body features of the MBS code SIMPACK (potentially to be combined by the substructure import feature FEMBS).

Concerning the physical aspects the aim has been the modelling of — beside the gyroscopic — the complete elastic and mass coupling including geometric stiffness terms necessary to map the linear stability behaviour of the rotating structure. The focus was put on the coupling mechanisms between the degrees of freedom by the influence of in particular the blade rotation.

With the convergence of eigenfrequencies of the analysed test blade cases areas of rotation speed have been identified where the offset coupled structure is extremely prone to interaction between the components of deformation from which the torsional deflection in terms of aeroelasticity seems to be the most relevant. Such gyroscopic resonance phenomena can be hazardous to flight safety since together with the aerodynamic forces acting on the blades they might enlarge the affinity of the rotor for aeroelastic instability.

Finally for validation purposes the results of the MBS code have been compared quantitatively to the results gained with the other method (FEM) as presented. The MBS results for the eigenfrequencies proved their compliance up to the numerical model accuracy (in the promille error range). Thus the potential of a sophisticated — and optionally hybrid — MBS code like SIMPACK as a powerful simulation tool for helicopter dynamics has been demonstrated with respect to the structural dynamics of the elastic rotor.

10 Symbols

u, v, w	Displacements of the beam cross sectional centre of gravity
α, β, γ	Rotations of the beam cross-section

x, y, z	Coordinates of the beam, with x being the longitudinal beam axis
η	Prandtl torsional coefficient ($\eta \rightarrow 1$ with $b/h \rightarrow \infty$)
n	Number of revolutions of the rotor
μ_x	Transversal mass distribution of the beam
$\hat{\mu}_h$	Rotational mass distribution of the beam
a_i	Proportionality factor for eigenvalue i
A	Index aerodynamic neutral axis
B	Index pitch axis
M	Index center of gravity
N	Index structural neutral axis
S	Index shear center

References

- [1] HOPKINS, A. STEWART; ORMISTON, ROBERT A.: *An Examination of Selected Problems in Rotor Blade Structural Mechanics and Dynamics*. American Helicopter Society, 59th Annual Forum, Phoenix, Az., May 6. – 8. 2003.
- [2] GASCH, ROBERT; KNOTHE, KLAUS: *Struktur-dynamik*. Vol. 1 and 2, Springer-Verlag Berlin, 1989.
- [3] FA. INTEC GMBH/SIMPACK AG: *SIMPACK Reference Guide and SIMDOC Manuals*. Vers. 8805 (8903), Munich, 8. Sept. 2007
- [4] JOHNSON, WAYNE: *Helicopter Theory*. Dover Publications, Inc., New York, 1994.
- [5] BIELAWA, RICHARD L.: *Rotary Wing Structural Dynamics and Aeroelasticity*. AIAA Educational Series, American Institute of Aeronautics and Astronautics, Wash., 1992.
- [6] WAITZ, STEFAN: *From FEM to MBS: Stability Analysis of the Elastic H/C-Rotor*. European Rotorcraft Forum 2010, Paper-Id. No. 107, Paris, 2010.